Improved of Load Frequency Control in a Three-Area Non-Reheat System Using Hybrid Fuzzy-PI Controller and PIDF based on Mountain Gazelle Optimizer

Abdulslam A. Aloukili*, Tarek M .Nasser**, Salama Abuzaid**, Mohammed A. Mehanna **

* Electrical Engineering Department, Faculty of Engineering, University Of Dernah, Dernah, Libya

**Electrical Engineering Department, Faculty of Engineering, Al-Azhar University, Cairo, Egypt

(a.alaokali@uod.edu.ly, Tarekmahmoudn1967@hotmail.com, Salama.ali@azhar.edu.eg, Mehanna@azhar.edu.eg)

‡Corresponding Author: Abdulslam .A. Aloukili, Tel: +218911075083

Received: 22.05.2023 Accepted:09.07.2023

Abstract- This research suggest a new load frequency control (LFC) system for a three-area non-reheat system. The system that is suggested employs a hybrid fuzzy-PI controller and Mountain Gazelle Optimizer (MGO), with Integral Time Absolute Error ITAE serving as the objective function. The proposed controller's performance is compared with different techniques including PID based on MGO, PID-based on transet search optimizer TSO, PID-based on Pelican Optimization Algorithm POA, fuzzy-TSO, and fuzzy-POA. The proposed hybrid fuzzy-PI controller with MGO performs better than the other controllers in terms of reduced settling time, maximum overshoot, maximum undershoot of frequancy deveation, and ITAE, according to the results. The effectiveness of the proposed controller is further verified in various scenarios, including sudden changes in loads and the incorporation of renewable energy sources (RESs), such as wind turbines and solar panels, along with energy storage systems. Overall, the findings show that the suggested controller is a successful method for enhancing frequency stability in a three-area non-reheat power system under a variety of operating scenarios. Matlab 2020 was used in this work.

Keywords: Load Frequency Control (LFC); Mountain Gazelle Optimizer; renewable energy sources (RESs); energy storage (ES); Integral Time Absolute Error (ITAE).

1. Introduction

The microgrid is a networked power generation system made up of several connected generators. Each area may contain more than one generator, including non-reheat turbines, thermal turbines, gas turbines, nuclear reactors, wind turbines, PVs, and others. All of these generators can be connected together in one or more areas. In the power system, strong generation control is always necessary, especially when renewable energy sources (RES) are widely utilized in utility systems. Increasing the RES in the utility makes the system have low inertia and weak ability to stand against sudden changes in loads or any disturbance in the system [1-3].

Many researchers have proposed several problems and techniques to achieve the maintenance of load frequency control. A strong Active Disturbance Rejection Control is recommended by others in [4] to enhance load frequency control in three areas: non-reheat, reheat, and hydraulic. Dekaraja in [1] studied the impact of storage systems in three area systems with integrated RES and AVR control. In [5], the authors proposed a hyped technique GA-PSO to improve PID controller for making the three-area system more robust. In order to enhance the load frequency control in three area systems, a FOPID controller was utilized in [6]. Zeynelgil in [7] used an artificial neural network to improve an integrated system with four areas. Also, the authors in [8] suggested a FOPID controller to enhance a four-area system integrated with RES. In [9], to optimize PID controller parameters, a fuzzy logic controller is used in conjunction with PSO. The load frequency control in the fore area system was improved by the authors in [10] using a firefly algorithm. ANFIS controller was used in [11] to improve the LFC combined with SMES-TCPS. A PI-PID cascade controller was used in [12], based on the Flower Pollination algorithm, to enhance LFC on the multi-area system. Improving the PID on LFC based on PSO with ANFIS was developed in [13]. Also, deep learning techniques were employed to improve generation control and reduce frequency deviation [14]. Real-time rotational inertia provision and frequency

deviation in power systems were both handled by predictive control [15]. In [16], the authors used a PI controller to improve generation control for a combined system of PV with a thermal system. Additionally, a PI controller uses two-area thermal power in the AC-DC tie-line [17]. Furthermore, the RESs' inconsistent and variable power generation leads to an unstable and inadequate power supply [1, 3, and 18]. To determine the ideal parameter for AGC for three areas, the authors in [19] develop a novel quasi-oppositional harmony search algorithm. [20] Uses a BFOA algorithm with the PSO for multi-objective LFC in hybrid power systems. Several other methods have been proposed to improve load frequency control in power systems [21–26].

This study will utilize a three-area non-reheat system that incorporates a PID controller with a derivative filter. The controller will be tuned using optimization techniques that are hybridized with a fuzzy logic PI controller. Energy storage systems such as SMEs and BES will support the non-reheat system, while RES like wind turbines and PV systems will be integrated into the system to assess the controllers' behavior. The Mountain Gazelle Optimizer, Pelican Optimization Algorithm, and Transit search are optimization techniques used in this research to obtain better PIDF parameters. The first section of this work introduces the study, while the second section describes and models the system. The third section discusses the study's control strategy, and the fourth section presents findings and discussions. The last section brings this work to a close.

2. System Description and Modeling

2.1 System Description

A three-area non-reheat thermal system is used in this study. Each area has a single generator, turbine, and governor, and is connected to loads and energy storage systems. Additionally, RES will be inserted into the system. Once the load increases or any fault occurs in the system that causes deceleration or acceleration of the frequency, the controller must adjust the system parameters to restore its stability. One turbine, one governor, and one generator are present in each of the three areas of the system depicted in Figure 1 single-line diagram. The ratings for areas one, two, and three are 2000MW each [27-30]. Energy storage elements are also inserted into the system to improve its performance. The system also includes RES as shown in the Figure 1.

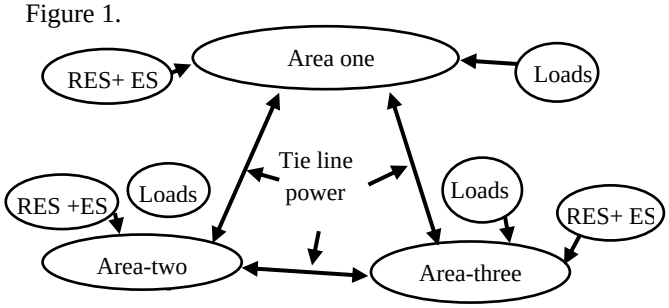

Fig 1: Simple three-area non-reheat system diagram

The p[illegible] system in[illegible] also, and the ximum power sharing in the tie-line is 200MW between each area. The frequency base factor B is 0.425 for each area. T_{12}, T_{23}, and T_{31} are the synchronizing coefficient between areas. The LFC Participation Factor a is equal to 1 for each area. K_{psi} is the gain of the power system. A first-order equation is represented by each load and generation block, as seen in Figure 2. Furthermore, first-order equations describing the governors and turbines are provided.

Table 1: Three area system parameters

Area	1	2	3
Speed regulation	R=2.4	R=2.4	R=2.4
tie max	200	200	200
Inertia constant	H=5	H=5	H=5
Base power	2000MW	2000MW	2000MW
Governor time constant	Tg=8e-2	Tg=8e-2	Tg =8e-2
Turbine time constant	Tt=0.3	Tt=0.3	Tt=0.3
K_{psi}	120	120	120
B	0.425	0.425	0.425
T_{ps}	20	20	20
a	1	1	1
$T_{12}=T_{23}=T_{31}$	.08674	.08674	.08674

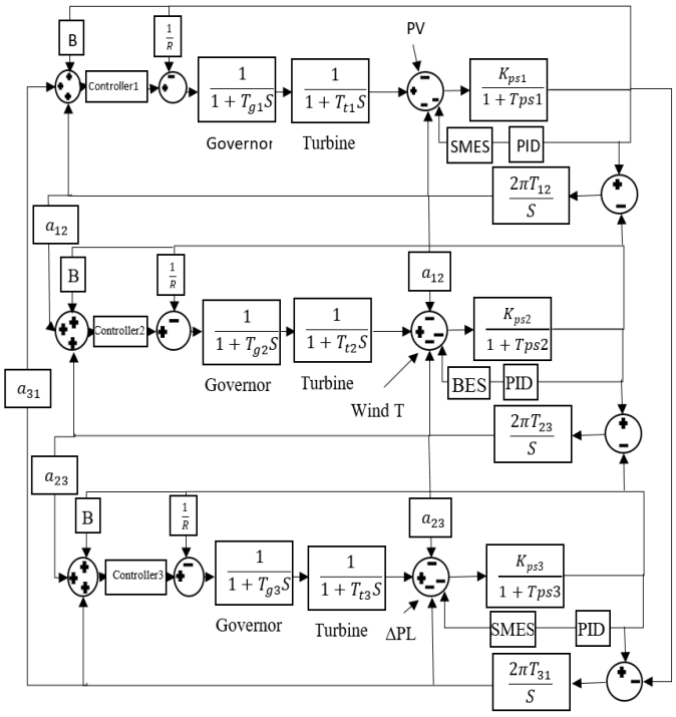

Fig.2: a single line diagram for a three-area non-reheat system that incorporates RES and energy storage

2.2 Problem Formulation

The goal of this article is to improve system stability, reduce overshoot, undershoot, and settling time by finding the best parameters for the controller. The objective function used in this article is ITAE (integral time absolute error), which is shown to be more effective than other approaches in [31]. ITAE minimizes the area control error (ACE) in each area, which is a function of the frequency deviation Δf and

the power tie-line ΔPtie between areas, such as area one and two. Equations (20-23) below define the objective function. Artificial intelligence (AI) will find the optimal parameters of PID controller after 1000 iterations. Three optimization techniques, MGO [32], POA [33], and TSO [34], are used alone and also combined with fuzzy-PI to enhance system performance. They are applied to find the optimal parameters of PID controller.

$$\text{ITAE}=\int_0^{\infty} t|ACE_1 + ACE_2 + ACE_3|dt \quad (1)$$

Where

$$ACE_1= \Delta f_1+\Delta P_{tie\ 12}+ \Delta P_{tie\ 31} \quad (2)$$

$$ACE_2= \Delta f_2+\Delta P_{tie\ 23}+ \Delta P_{tie\ 12} \quad (3)$$

$$ACE_3= \Delta f_3+\Delta P_{tie\ 23}+ \Delta P_{tie\ 31} \quad (4)$$

2.3 Modeling of RES and ES Systems

SMES model : A type of energy storage known as superconducting magnetic energy storage (SMES) uses the magnetic field produced by a superconducting coil to store energy. SMES systems employ high-temperature superconductors to produce a powerful magnetic field when an electric current flows through the coil. The stored energy can then be released by reversing the current flow, enabling the rapid discharge of significant amounts of energy. SMES systems are frequently utilized in applications such as power grid stabilization, peak shaving, and load leveling [1, 3, 18, 35]. Calculations for power (P) and magnetic energy (E) are as follows:

$$E = 0.5LI^2 \quad (5)$$

$$P = \frac{\partial E}{\partial t} = LI\frac{\partial I}{\partial t} = VI \quad (6)$$

In this study the SMES system used as first-order transfer function[1,3].

$$G_{SMES} = \frac{K_{SMES}}{1+T_{SMES}S} \quad (7)$$

where gain K_{SMES}=0.98 , time constant T_{SMES}= 0.03s

BES model: Battery energy storage is a technology that transforms chemically produced energy from renewable sources like solar and wind into electrical energy and stores it in batteries for later use. This technology is becoming increasingly important as the world moves towards a more sustainable energy future. Battery energy storage can help reduce the need for traditional power plants, reduce emissions, and provide backup power during outages. Additionally, it is able to store additional energy produced by renewable resources for later use when demand is higher. A first-order equation will be used to represent the BES in this study, which will use fast response types of BES devices [1,3,18,36]:

(8)

W here gain K_{BES} = 1.8 , time constant T_{BES}= 0

$$G_{BES} = \frac{K_{BES}}{1+T_{BES}S}$$

PV model: One of the sources of renewable energy is solar power. The PV array's output power can be calculated using the formulas below [3,18,36], where they depend on solar radiation and array temperature.

$$P_{Pv} = P_{Pv.STc} \times \frac{G}{G_{STC}} \times (1 + \alpha(T_a - T_{STC})) \times \eta_{MPPT} \quad (9)$$

Where

STC is the stander test conditions
$P_{pv.STC}$: the related output power
G_{STC}: solar irradiance STC (1000W/m^2)
T_{STC}: reference temperature (25°C)
η_{MPPT}: Maximum power point tracking
α: temperature coefficient

In this work, the photo voltaic data is taken from a real photo voltaic system in dernah, Libya where the maximum radiation is 980 W/m^2. The maximum power point tracking was 98%. Consuming the surrounding temperature constant of 25°C [3]. Consequently, during the radiation G, the PV array's output power changes. Therefore the PV model can be written as below:

$$P_w = \frac{\Delta P_{PV}}{\Delta G} = \frac{K_{Pv}}{1+T_{pv}s} \quad (10)$$

While

K_{pv} =1 is the gain and T_{pv}= 0.03s is the time constant

Wind turbine model: One of the RES, the wind turbine's output power is determined by the wind speed acting on its rotor and can be calculated using the equation below [3,18.36]:

$$P_w = 0.5 \times \rho \times A \times C_p(\lambda.\beta) \times V^3 \quad (11)$$

In Equation 11, ρ represents air density, A represents rotor speed swept area, and V3 represents the wind speed. The power coefficient, or Cp, depends on the tip speed ratio λ and blade pitch angle β. To ensure that the wind turbine operates at its best, the power coefficient Cp is typically controlled at low and medium wind speeds. The wind speed used in this study was gathered from a real wind project in Libya's Dernah city. Changes in output power can be expressed as a first-order equation as shown below for small signal stability in the system:

$$G_{wt} = \frac{\Delta P_{WTG}}{\Delta P_W} = \frac{K_{WTG}}{1+T_{WT}S} \quad (12)$$

Where the gain of K_{WTG} = 1 ,with a time constant T_{WT} = 1.5

3. Control Strategy

The control strategy proposed in this article is a hybrid controller that combines a PIDF is a PID controller with a derivative filter, additionally, PI controller based on fuzzy logic controller [37-40]. The PID parameters are tuned using the mountain gazelle optimizer (MGO). Additionally, other PID controllers are integrated into storage energy systems to enhance system performance. The Figure below illustrates FPI-PID.

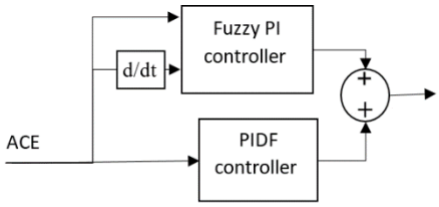

Fig. 3: Fuzzy PI-PID controller

To achieve better outcomes and performance, a PID controller with a derivative filter will be used. To lessen the noise signal, the value of this filter can be changed. A PID controller with a filter is shown in Figure 4 below.

$$U_{PID}(t) = K_p e(t) + K_i \int_0^t e(t)\ dt + K_d \frac{N}{1+N\frac{1}{s}} \quad (13)$$

The proportional, integral, derivative, and filter parameters will be obtained by an MGO

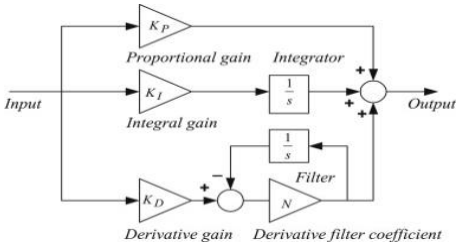

Fig. 4: shows below the PID controller with filter

3.1 Fuzzy-PI Controller

A fuzzy PI controller is a type of control system that uses fuzzy logic and proportional-integral (PI) control to regulate the behavior of a system. It combines the advantages of both fuzzy logic and PI control to provide an efficient and robust control solution. The fuzzy PI controller uses fuzzy logic to determine the appropriate output for a given input, while the PI controller adjusts the output based on the error between the desired output and the actual output. This combination allows for more accurate control than either method alone [40-42].

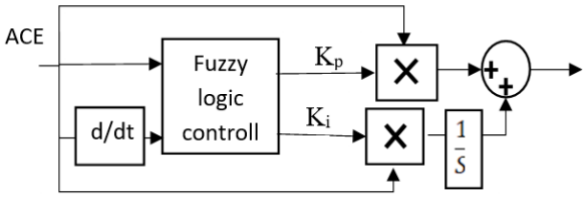

Fig .5: Fuzzy logic control PI

In this article, online tuning for a PI controller is achieved by using a fuzzy logic controller, which determines the best parameters for the PI controller.

The Fuzzy Logic Controller (FLC) is a system that uses fuzzy logic to process input data and produce an output. It consists of four main components: fuzzification, a Fuzzy Inference System (FIS), a rule-based system, and defuzzification. Before the input data is sent to the fuzzification process, it must be preprocessed by normalizing or scaling the measurement quantities. This preprocessing step transforms the crisp value into a fuzzy set, which is then used by the FIS to execute all reasoning schemes and generate an output. Finally, the output is defuzzified to obtain a crisp value. Membership functions (MFs) such as Gaussian, bell-shaped, trapezoidal, and triangular are used to design a Fuzzy Logic Controller (FLC). Tuning fuzzy control is a difficult task that involves rule tuning and MFs tuning, which may not be effective. To obtain an optimum and robust FLC, the system's parameters have been tuned. However, for real-time applications, symmetrical triangular MFs (STMFs) are preferred due to their simplicity compared to other MFs. The rule base of an FLC is composed of membership functions and control rules. The output of the FLC is a fuzzy set that needs to be transformed by a defuzzification scheme into a numeric value. Due to this study's focus on defuzzification schemes, five triangular MFs are utilized. These five MFs were selected using five linguistic variables, which include the input and output of FLC for negative large (NL), negative small (NS), zero (ZE), positive small (PS), and positive large (PL). The input/output MFs of the FLC are shown in Figure 6. The 25 rule two-dimensional rule-base for ACE, dACE, and FLC output is shown in Table 2. This study employs Mamdani and centroid methods for FIS and defuzzification, respectively [43-46].

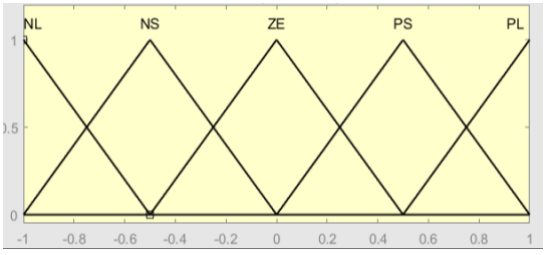

Fig. 6: membership function MF of input/output of the fuzzy logic controller

The two input signals to the FLC are ACE and the derivative of ACE (dACE), and the output from the controller is a real-time value for Kp and Ki. The mathematical expression of output values is based on Table 2

Kp= fp (ACE, dACE) , Ki= fi (ACE, dACE) (14)

Table 2: Fuzzy rule for outputs/inputs fuzzy logic controller [1,38]

	dACE				
ACE	NL	NS	ZE	PS	PL
NL	NL	NL	NL	NS	ZE
NS	NL	NS	NS	ZE	PS
ZE	NL	NS	ZE	PS	PL
PS	NS	ZE	PS	PS	PL
PL	ZE	PS	PL	PL	PL

3.2 Mountain Gazelle Optimizer MGO

The Arabian Peninsula and its environs are home to the Mountain Gazelle species of gazelle. Although it is widely distributed in these areas, Because of its close resemblance to Robinia tree, its density is extremely low. Due to Gazella bennettii, the species lost some of its territory, a species better suited to surviving in hot climates, as temperatures increased in the late Holocene. The Mountain Gazelle is fiercely territorial, and their territories are spread far apart from one another. Mother-offspring herds, young male herds, and single males' territories are the three main groups they form. The struggle between nearby males for control of their environment is less violent and more dramatic than the conflict between male gazelles for the ownership of females. Compared to adult males or owners of land more young males use their horns in combat. The mountain gazelle is a migratory animal that often travels over 120 km in search of food. It can run for quite a distance at an average speed of 49 miles per hour, which is an incredibly fast speed [32].

To create a mathematical representation for its operations, the Mountain gazelle optimizer algorithm draws on the dynamic in society and groups of mountain gazelles. The four main aspects of a mountain gazelle's life are taken into account in this model: solitary territorial males, maternity herds, bachelor male herds, and food migration[32].

Territorial Solitary Males

Male mountain gazelles establish their own solitary territories when they are mature and physically capable, and they fiercely defend them. These territories can be quite far apart from one another, and battles between adult males often occur over the possession of a female. While older males work to protect their territory, younger males try to conquer it or the female. Figure 7 depicts a high-level view of the MGO agent-based optimization approach.

$$TSM = male_{gazelle} - |(r_{i1} \times BH - r_{i2} \times X(t)) \times F| \times Cof_r \quad (15)$$

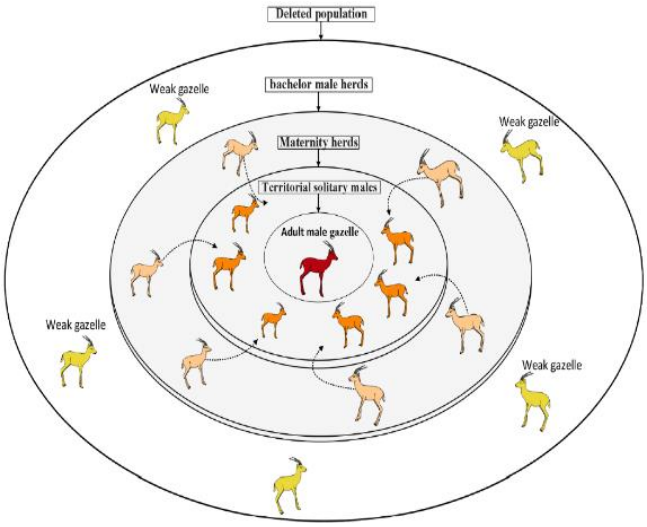

Fig. 7: Description of the improvement approach based on agents of MGO

In equation 15, $male_{gazelle}$ is a position vector that represents the ideal worldwide solution, r_{i1} and r_{i2} are random integers, BH is the coefficient vector of young male herd calculated by equation 16, additionally, to improve search efficiency, Cofr is a coefficient vector that is randomly chosen and updated after each iteration. Equation 14 allows for its calculation.

$$BH = X_{ra} \times \lfloor r_1 \rfloor + M_{pr} \times \lceil r_2 \rceil,\ r_a = \{\lceil N/3 \rceil \ldots N\} \quad (16)$$

The random solution (young male) within the range of ra is represented by X_{ra}. N is the total number of gazelles, Mpr is the typical number of search agents (N/3) that were randomly chosen. R1 chosen as random value also R2.

$$F = N_1(D) \times \exp\left(2 - Iter \times (2 / Max_{Iter})\right) \quad (17)$$

$$Cofr = \begin{cases} (a + 1) + r_3, \\ a \times N_2(D), \\ r_4(D), \\ N_3(D) \times N_4(D) 2 \times \cos((r_4 \times 2) \times N_3(D)) \end{cases} \quad (18)$$

The amplitude (a) of Cofr is calculated by using this equation:

$$a = -1 + Iter \times (-1 / MaxIter) \quad (19)$$

In equations 17 & 18, N1 is a selected randomly from the normal numbers. Max_{Iter} represents the total number of iterations, while Iter represents the current iteration. Additionally, r_3, r_4, and rand are arbitrary numbers from 0 to 1. N_2, N_3, and N_4 are arbitrary numbers that fall within the

parameters and bounders of the problem. r_4 is a random value that falls between 0 and 1 in the problem dimensions. Cos represents the cosine function, and that's all.

Maternity Herds

The life cycle of mountain gazelles depends on maternity herds because they offer a secure environment for female gazelles to give birth to robust male gazelles. By vying for females and helping to deliver young, male gazelles also contribute to the reproduction process. This behavior is formulated using.

$$MH = (BH + Cof_{1,r}) + (r_{i3} \times male_{gazelle} - r_{i4} \times X_{rand}) \times Cof_{1,r} \quad (20)$$

In equation 20 BH Using equation 16, represents the vector of impact factors for young males. $Cof_{2,r}$ and $Cof_{3,r}$ are coefficient vectors randomly chosen and independently calculated using eq.18. r_{i3} and r_{i4} are random integers between 1 and 2.In the current repetition, $Male_{gazelle}$ represents the best overall solution for adult males. X_{rand} represents the gazelle's position along its vector that was randomly chosen from the entire population.

Bachelor Male Herds

The male gazelles establish their own territories and attempt to gain control of female gazelles after they reach maturity. This often leads to confrontations between young and older males, which can result in violent behavior.

$$BMH = (X(t) - D) + (r_{i5} \times male_{gazelle} - r_{i6} \times BH) \times Cofr \quad (21)$$

In the current iteration, the gazelle vector's position is represented by X(t), and D is calculated using the equation 22. r_{i5} and r_{i6} are random integers between 1 and 2 that are random values. $Male_{gazelle}$ depicts the location of the male gazelle's vector (the ideal solution). The young male herd's impact factor, BH, is also determined by using equation 16.

$$D = (|X(t)| + |male_{gazelle}|) \times (2 \times r_6 - 1) \quad (22)$$

In the most recent iteration, X(t) and $male_{gazelle}$ represent the positions of the gazelle vectors, respectively. The adult male (best solution) is also calculated by the location of the vector. Additionally, r_6 is a random value from 0 to 1.

Migration to Search for Food

Mountain gazelles are always on the move in search of food, migrating over long distances. They possess great agility and strength, enabling them to run fast and jump high. The equation below mathematically formulates this technique of gazelle movement. Figure 8 shows the MGO flow chart.

$$MSF = (ub - lb) \times r_7 + lb \quad (23)$$

In equation 23, The upper and lower bounds, respectively, are represented by ub and lb. r_7 is an integer number amidst 0 and 1 that is randomly chosen [32].

4. Results and Discusses

The performance of the three-area non-reheat system is evaluated based on system stability, reduction of overshoot and undershoot, and settling time. Two types of controllers were used: PID and hybrid fuzzy PI-PID with different optimization algorithms under several scenarios. The PID controller parameters will be selected using optimization techniques such as MGO, POA, and TSO. The Fuzzy PI controller parameters will be calculated and changed instantly by the controllers depending on system requirements.

Case study one involves studying the system performance under several load conditions (dynamic loads). In this case study, dynamic load conditions will be applied to each area of the three-area non-reheat system as shown in Figure 9.

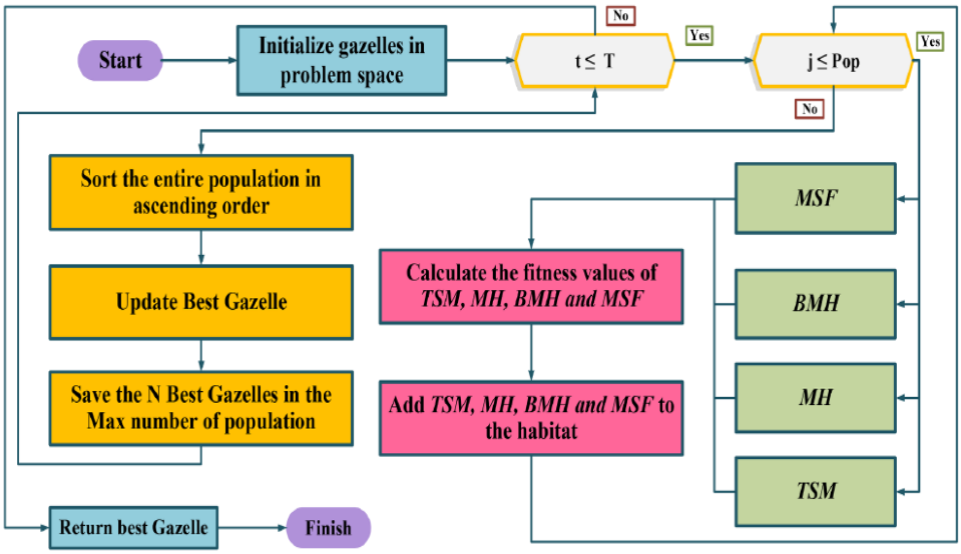

Fig. 8: flow chart of MGO[35]

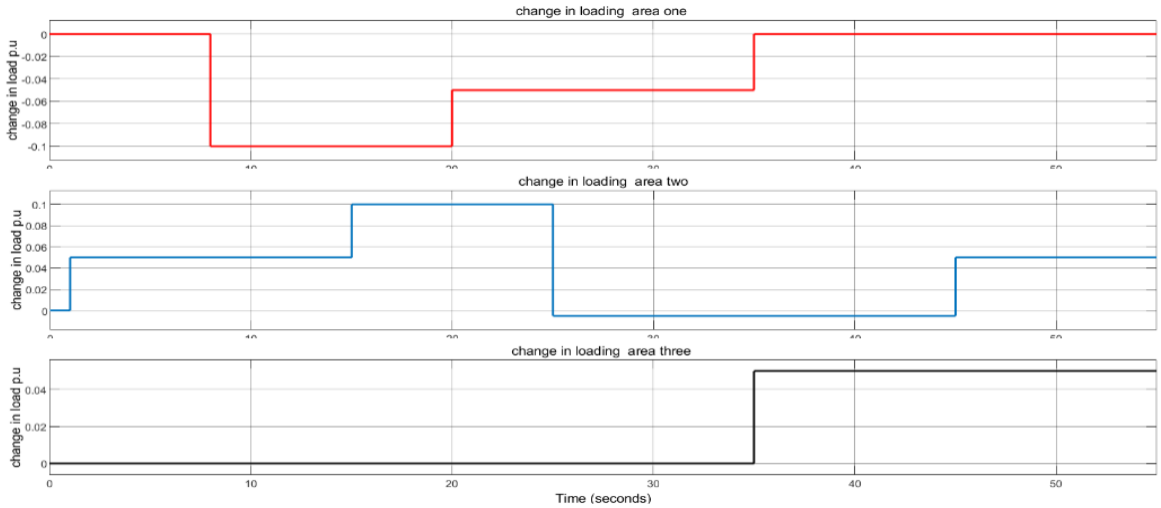

Fig. 9: load change in each area for a three-area non-reheat system

According to the changes in loads shown in Figure 9, the response of Area One is presented in Figure 10(a-g). Load changes occurred multiple times in Areas One and Two, with a single change in Area Three to test the controller's performance. The controllers were designed to minimize frequency deviation. Figures 10(a-g), 11(a-g), and 12(a-g) demonstrate the controllers' performance, with fuzzy-MGO proposing the best response due to its shorter settling time, absence of system oscillations, and lower steady-state error.

This is also reflected in Table 3's ITAE values. Overall, fuzzy-MGO and MGO demonstrated superior performance even in Area Three. Fuzzy-POA, POA, fuzzy-TSO, and TSO exhibited significant oscillations and took five seconds to reach steady-state error in Area Three. Fuzzy-MGO and MGO both proposed the best performance with no oscillations observed in Δf1, Δf2, Δf3 or the power tie-line. According to maximum over-shoot (MOS), maximum under-shoot (MUS), settling-time (ST), and ITAE values, Tables 4, 5, and 6 compare the proposed techniques.

Table 3: PID controller parameters in each area with ITAE in each case

Technique	ITAE PID	ITAE Fuzzy-PID	Controller	Area	K_p	K_i	K_d	N
MGO	0.1123	0.0707	System controller	1	299.956	249.999	69.916	502.177
				2	299.784	250.000	69.967	1319.184
				3	275.711	249.978	68.788	836.392
			Energy storage controller	1	47.122	54.451	2.158	1945.914
				2	0.164	100.000	1.683	31.294
				3	0.088	0.139	0.329	434.140
POA	0.1741	0.1131	System controller	1	300.000	249.057	59.546	1941.502
				2	291.796	142.718	67.750	1998.960
				3	253.381	249.896	54.766	1933.164
			Energy storage controller	1	97.953	99.679	30.914	1926.859
				2	100.000	95.236	34.071	1993.496
				3	7.894	94.802	0.000	1309.885
TSO	0.1419	0.0948	System controller	1	299.997	236.712	70.000	1995.108
				2	299.984	250.000	56.868	1309.889
				3	205.316	198.464	65.457	701.346
			Energy storage controller	1	76.333	84.257	5.586	1999.967
				2	0.000	100.000	9.291	1759.810
				3	42.523	85.311	38.373	0.000

Table 4: Comparison between the proposed techniques in are one MOS, MUS, and ST

Tech	sec	MOS	MUS-	ST	Tech	MOS	MUS-	ST
Fuzzy - MGO	1	1e-5	1.25e-4	3.5	MGO	1.2e-5	1.4e-4	4
	8	14.8e-4	1e-4	3		14.9e-4	2e-4	4
	15	0.15e-4	1.25e-4	3.5		0.12e-4	1.4e-4	4
	20	0.2e-4	6.9e-4	3		0.17e-4	6.92e-4	3.2
	25	2.7e-4	0.2e-4	3.5		2.9e-4	0.15e-4	4
	35	0	6.9e-4	2.5		0	6.92e-4	3
	45	1.3e-5	1.25e-5	3.5		1.2e-6	1.4e-5	4
Fuzzy -POA	1	1.2e-4	0.51e-4	5	POA	1.2e-4	0.26e-4	5
	8	3.85e-4	0.4e-4	7.2		4.1e-4	0.4e-4	6
	15	1.2e-4	0.51e-4	5		1.2e-4	0.26e-4	5
	20	0.4e-4	1.9e-4	5		0.4e-4	2.09e-4	5
	25	2.4e-4	1.2e-4	6		2.3e-4	0.65e-4	6
	35	0.4e-4	1.3e-4	6		0.15e-4	1.5e-4	6
	45	1.2e-5	0.51e-5	5		1.2e-5	0.26e-5	5
Fuzzy -TSO	1	0.61e-4	1.3e-4	4.5	TSO	0.38e-4	1.4e-4	4.5
	8	6.25e-4	2.3e-4	3		6.3e-4	2.1e-4	3
	15	0.61e-4	1.3e-4	4.5		0.38e-4	1.4e-4	4.5
	20	2.23e-4	3.2e-4	3		2e-4	3.21e-4	3
	25	3.65e-4	1.24e-4	4		3.75e-4	0.8e-4	4
	35	0	3.2e-4	3.4		0	3.21e-4	3.4
	45	0.61e-5	1.3e-5	4.5		0.38e-5	1.4e-5	4.5

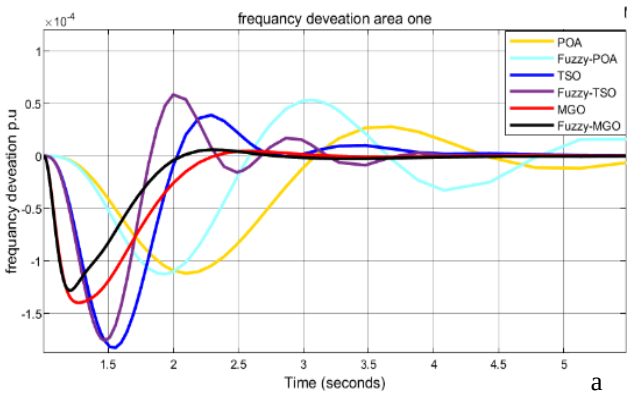

a

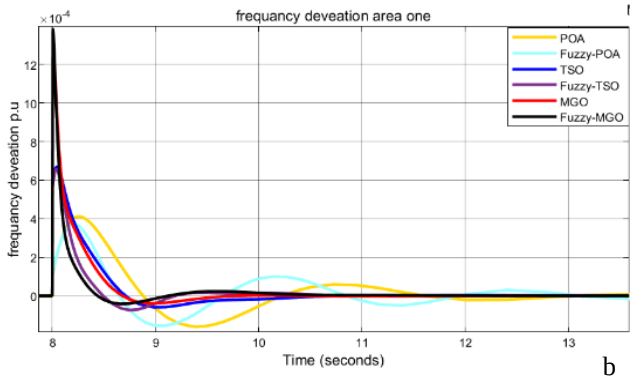

b

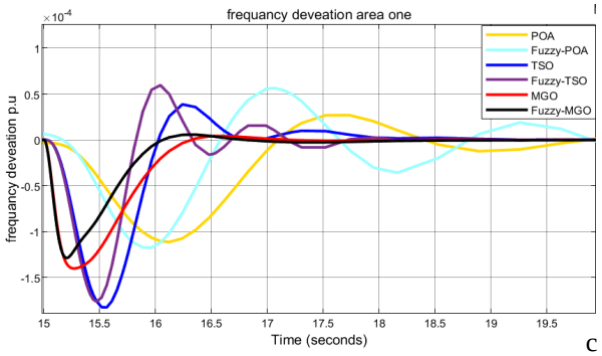

c

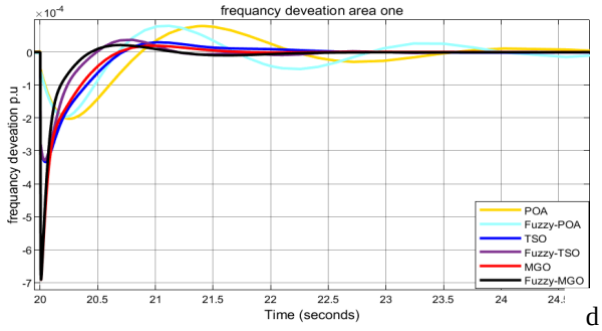

d

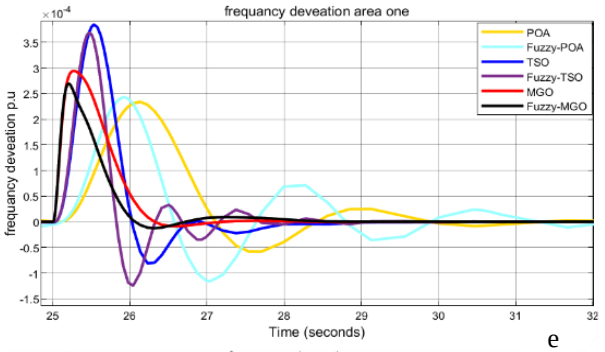

e

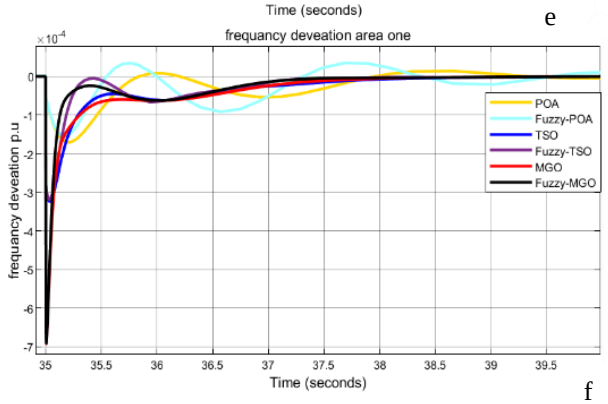

f

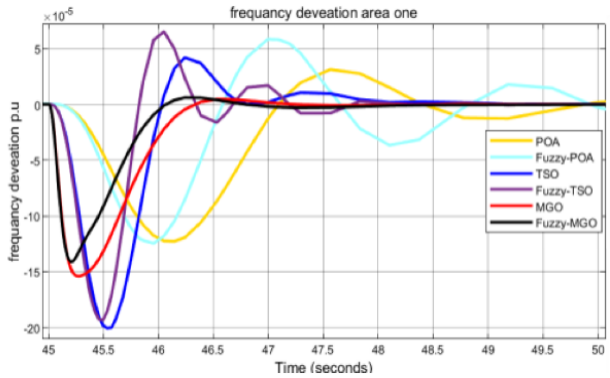

g

Fig. 10 (a-g): frequency deviation in area one with dynamic load change

Table 5: Comparison between the proposed techniques in area two MOS, MUS, and ST

Tech	sec	MOS	MUS-	ST	Tech	MOS	MUS-	ST
Fuzzy -MGO	1	0.22e-4	6.8e-4	3	MGO	0.2e-4	6.8e-4	3
	8	13e-5	7.4e-5	5		18e-5	7.5e-5	5.2
	15	0.22e-4	6.8e-4	3		0.2e-4	6.8e-4	3
	20	3.7e-5	6.1e-5	3.5		3.8e-5	8.9e-5	4
	25	13.6e-4	1e-5	3		13.8e-4	0.8e-5	3.2
	35	0	1.48e-4	3		0	1.9e-4	3.2
	45	0.22e-4	6.8e-4	3		0.2e-4	6.8e-4	3
Fuzzy-POA	1	0.4e-4	1.2e-4	5	POA	0.2e-4	1.3e-4	5
	8	13e-5	3.2e-5	6		12e-5	2.2e-5	6
	15	0.4e-4	1.2e-4	5		0.2e-4	1.3e-4	5
	20	2.1e-5	6.2e-5	5		1e-5	6.1e-5	5
	25	2.4e-4	2e-4	5		2.5e-4	1e-4	5
	35	0.35e-4	1.19e-4	6		0.2e-4	1.2e-4	6
	45	0.4e-4	1.2e-4	5		0.2e-4	1.3e-4	5
Fuzzy-TSO	1	2.9e-4	3.8e-4	4.5	TSO	2.7e-4	4.1e-4	4.5
	8	18e-5	8e-5	5		17e-5	8.1e-5	5
	15	2.9e-4	3.8e-4	4.5		2.7e-4	4.1e-4	4.5
	20	4.1e-5	9.2e-5	4.5		3.9e-5	8.5e-	4.5
	25	7.5e-4	6.2e-4	4		8e-4	5e-4	4
	35	0.1e-4	1.8e-4	4		0	2e-4	4
	45	2.9e-4	3.8e-4	4.5		2.7e-4	4.1e-4	4.5

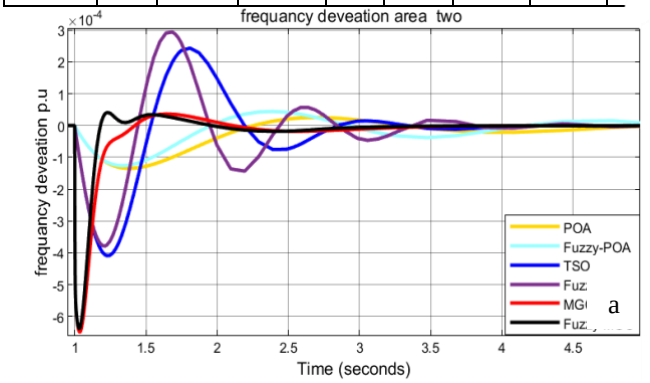

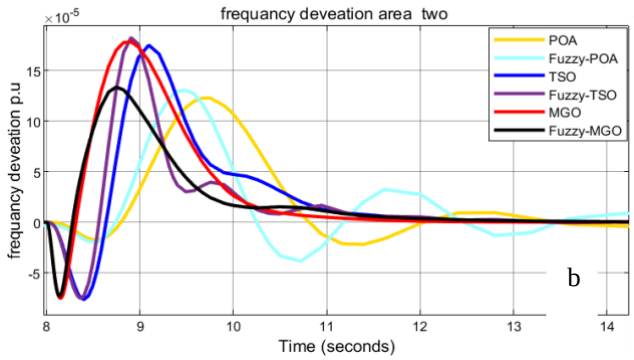

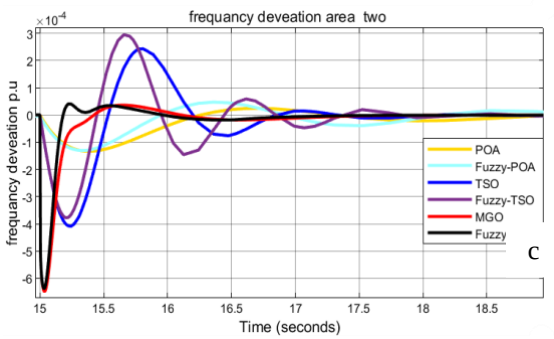

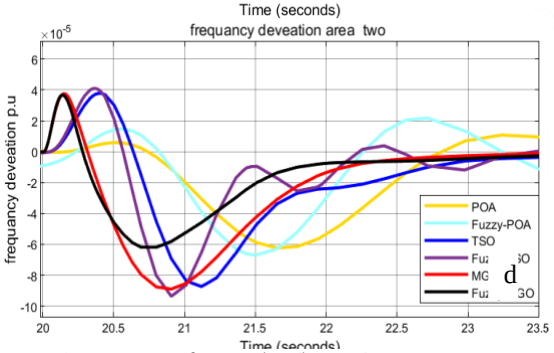

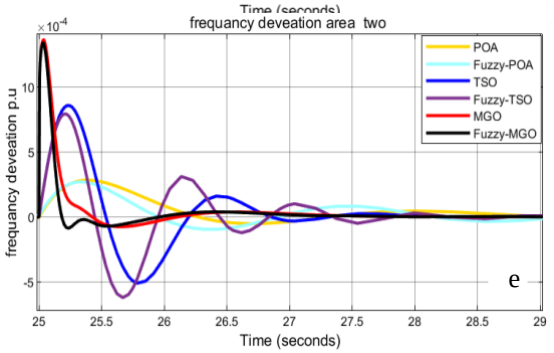

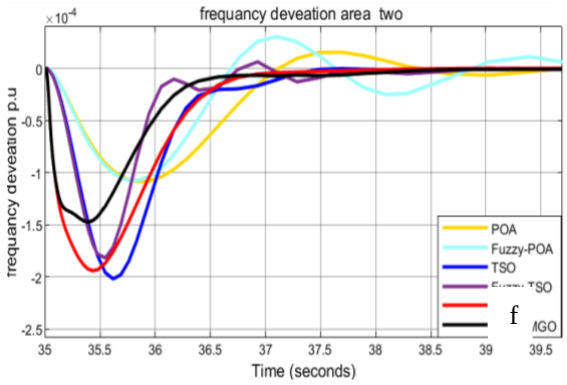

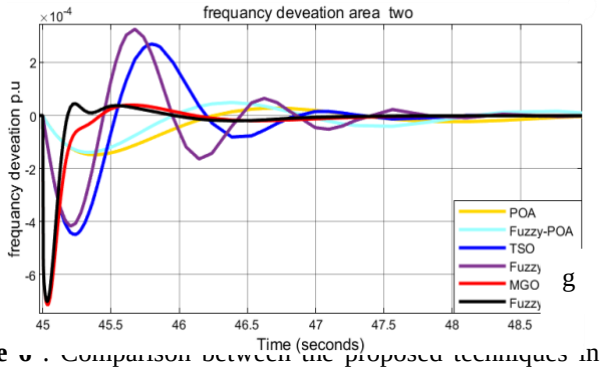

Fig. 11 (a-g): frequency deviation in area two with dynamic load change

MOS, MUS, ST and ITAE

Tech	sec	MOS	MUS-	ST	Tech	MOS	MUS-	ST
Fuzzy-MGO	1	6e-5	7.7e-5	3.4	MGO	6.2e-5	9.6e-5	3.7
	8	2.6e-4	0.2e-4	3		3.6e-4	0.5e-4	5
	15	6e-5	7.7e-5	3.4		6.2e-5	9.6e-5	3.7
	20	1.5e-5	12e-5	3		2.7e-5	18e-5	3.2
	25	16e-5	12e-5	3.3		21e-5	14e-5	3.6
	35	2e-3	2.9e-3	3		1.4e-3	2.95e-3	3.2
	45	6e-5	7.7e-5	3.4		6.2e-5	9.6e-5	3.7
Fuzzy-POA	1	2.4e-5	8e-5	5	POA	2.5e-5	8e-5	5
	8	2.25e-4	1e-4	5		2.7e-4	1.2e-4	5
	15	2.4e-5	8e-5	5		2.5e-5	8e-5	5
	20	5e-5	12e-5	5		5.5e-5	14e-5	5
	25	1.9e-4	0.6e-4	6		1.7e-4	0.6e-4	6
	35	3e-3	4e-3	6		3e-3	4e-3	6
	45	2.4e-5	8e-5	5		2.5e-5	8e-5	5
Fuzzy-TSO	1	4.8e-5	12e-5	5	TSO	5.5e-5	11.5e-5	5
	8	1.8e-4	.08e-4	3		2.3e-4	0.2e-4	5
	15	4.8e-5	12e-5	5		5.5e-5	11.5e-5	5
	20	1e-5	9e-5	5		2e-5	12e-5	5
	25	22e-4	1e-4	4		22e-4	1.1e-4	4
	35	1.9e-3	2.8e-3	5		1.9e-3	2.8e-3	5
	45	4.8e-5	12e-5	5		5.5e-5	11.5e-5	5

c

d

e

a

f

b

g

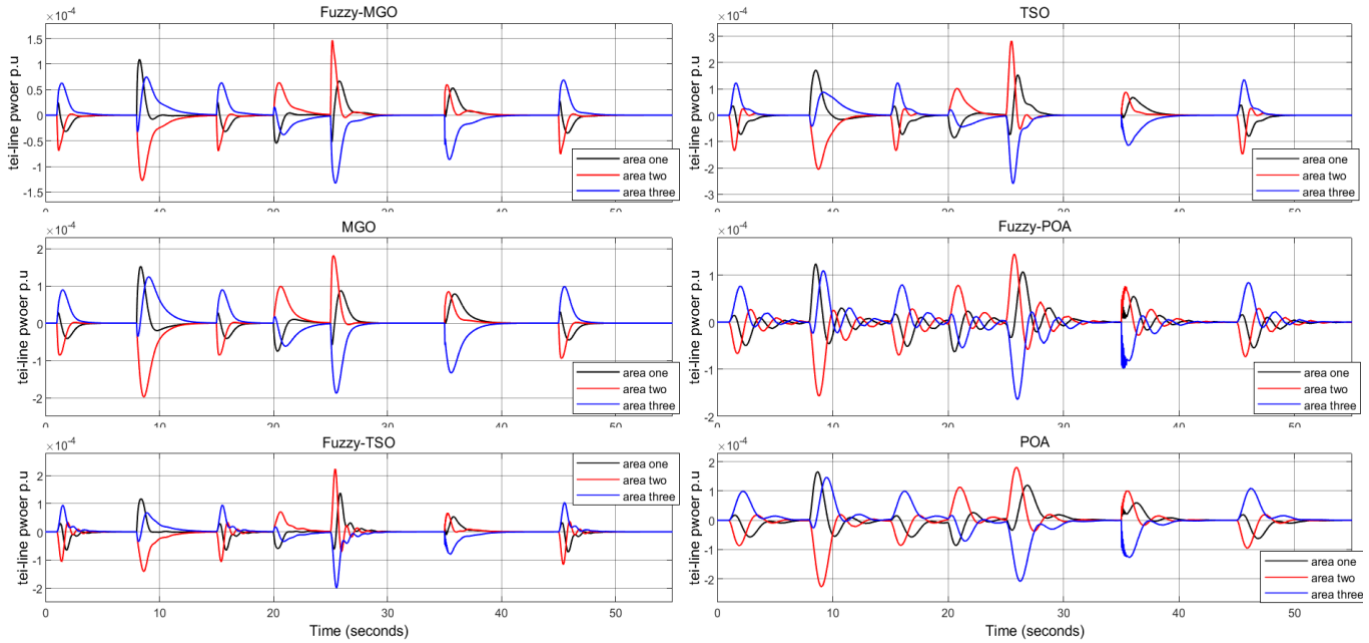

Fig. 13: power tie-line between areas one, two, and three

Case study two examines the performance of a controller with the penetration of RES. This section of the research explores the system's response to the unpredictable combination of hybrid renewable energy sources and dynamic loads, taking into account real-world wind, load, and solar irradiance data. Figure 14 illustrates the fluctuations in wind speed at the University of Derna Research Center in Libya on 21-10-2019, ranging from 5.9 to 12 m/s. The power output of a wind turbine in Area 1 varies between 0.1 to 0.15 p.u.

Solar irradiance data was also collected from the center of research at the University of Derna in Libya, showing a normal distribution of solar irradiance from six clock in the day to six clock in the night with a maximum of 980 W/m^2.Figure 14 also highlights PV power variation in Area 2, with a maximum of 0.25 p.u. lastly, a single day's worth of load change was predicted (Thursday) in Derna city, Libya. Taken together, these hybrid energy sources and dynamic loads provide valuable insight into the system response of renewable energy sources in different regions.

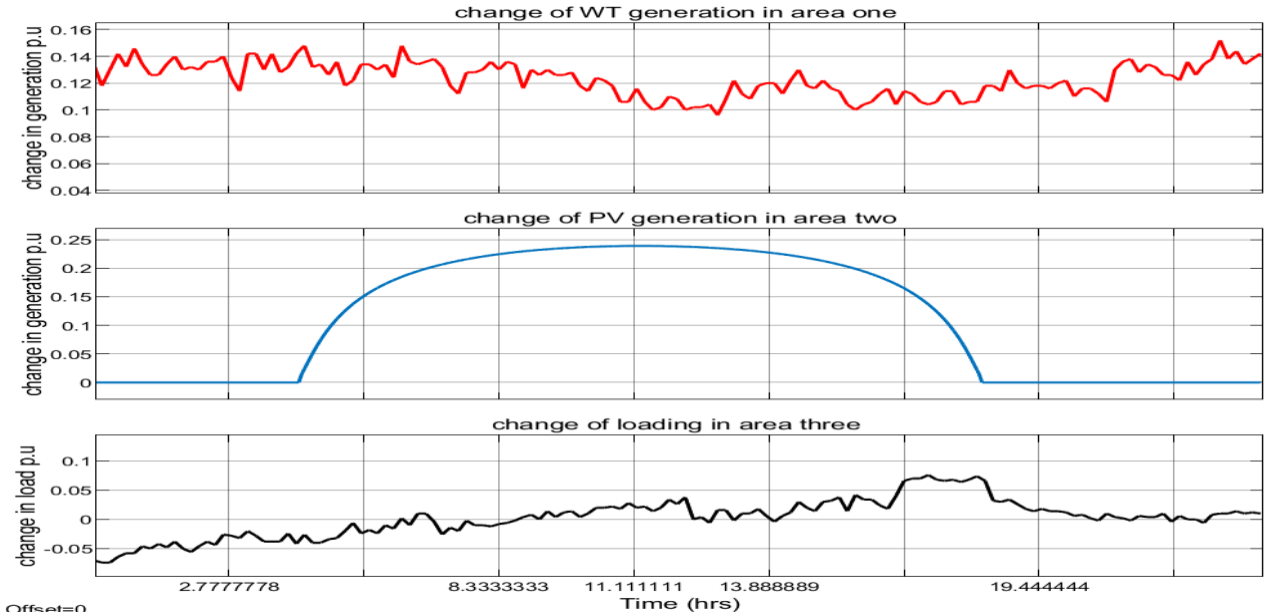

Fig. 14: change of generation and loading in areas one, two and three

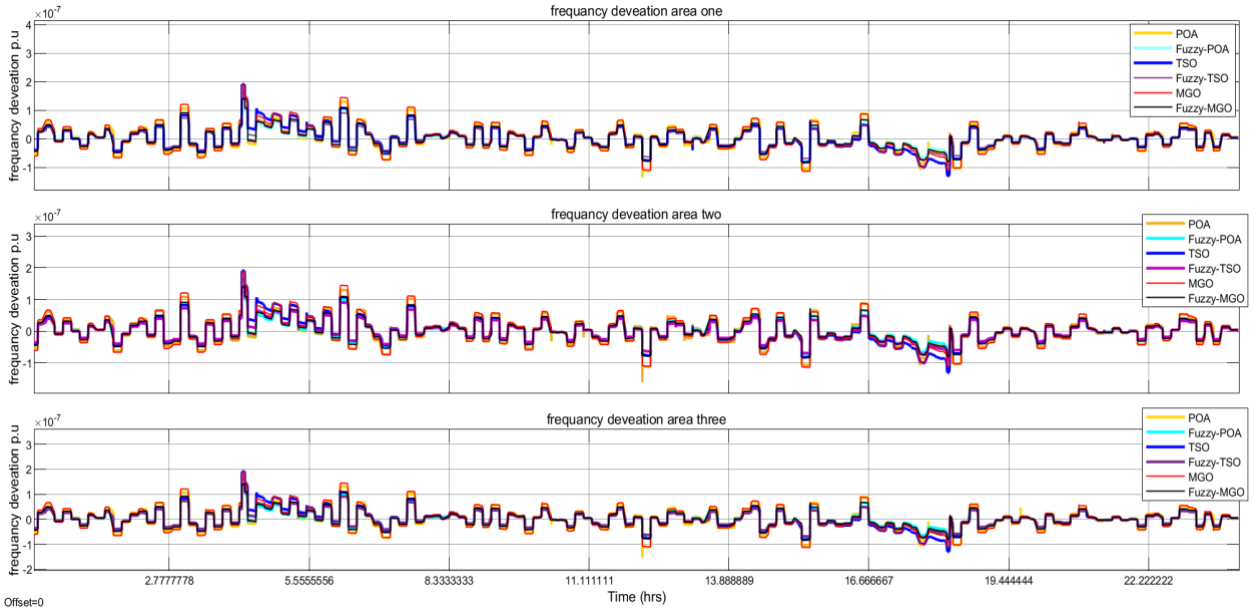

Fig. 15: frequency deviation in area one, two and three with RES and dynamic

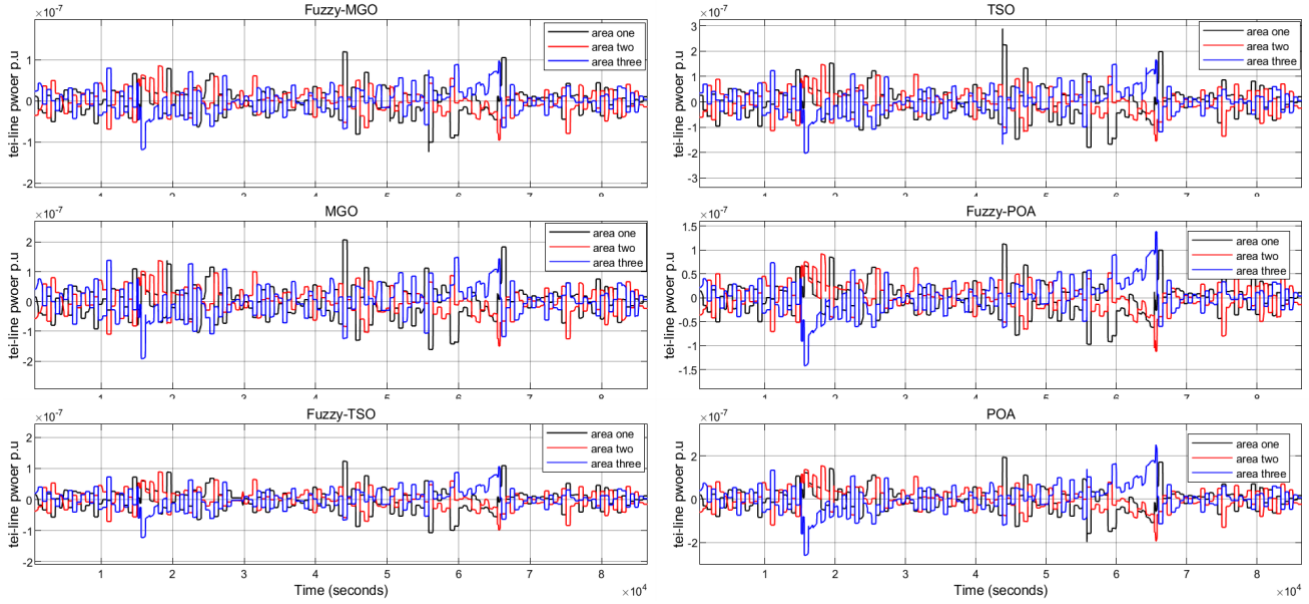

Fig. 16: power tie-line between areas for tech techniques

Figure 15 shows the system performance after inserting RES and dynamic load in areas one, two, and three. Also, Figure 16 show the power tie-line between areas. According to the Figures (15-16) Fuzzy-MGO and Fuzzy-TSO proposed best response than other techniques where has less oscillation, faster settling time, and less ITAE than other techniques. Where the ITAE for each method was: Fuzzy-MGO=651.2, Fuzzy-TSO=677.3, Fuzzy-POA=701.4, MGO=1062, TSO=1116 and POA=1129

5. Conclusion

The aim of this study is to propose a new and improved Fuzzy-MGO controller for a hybrid microgrid system that uses real data on wind speed and irradiance along with dynamic load changes from solar and wind energy sources. The controller also accounts for energy storage systems. The heuristic algorithm MGO is used to optimize the scaling factors and output gains also the membership function boundaries for the fuzzy-MGO controller. The effectiveness of the controller is compared with other controllers such as MGO-PID, Fuzzy-POA, Fuzzy-TSO, TSO-PID, and POA-PID. Moreover, various scenarios are run to test the resiliency and sensitivity of the controller to different step load perturbations, and uncertainties related to renewable energy sources such as wind speed fluctuations, solar irradiance variations, and load changes. When compared to the other controllers, the proposed Fuzzy-MGO controller performs better. In the first scenario, the system was tested under several loading conditions. Fuzzy-MGO showed the best performance, with a better settling time, minimal oscillation, and the lowest ITAE out of the other controllers. For the second scenario, renewable energy sources (RESs) were included in areas one and two, and area three saw a dynamic load for a full day. Fuzzy-MGO had the lowest

frequency deviation, fastest settling time, and lowest ITAE from the other controllers.

References

[1] B. Dekaraja, L. Saikia "Impact of energy storage and flexible alternating current transmission devices in combined voltage and frequency regulation of multiarea multisource interconnected power system". Energy Storage. 2022; 4(3):e317. (Article)

[2] M. Mokhtar, M. Marei, Mariam A. Sameh, M. Attia An Adaptive Load Frequency Control for Power Systems with Renewable Energy Sources". Energies 2022, 15, 573. (Article)

[3] A. H. Yakout, H. Kotb, H. M. Hasanien and K. M. Aboras, "Optimal Fuzzy PIDF Load Frequency Controller for Hybrid Microgrid System Using Marine Predator Algorithm," in IEEE Access, vol. 9, pp. 54220-54232, 2021, (Article)

[4] L. Dong, Yao Zhang, Zhiqiang Gao, "A robust decentralized load frequency controller for interconnected power systems", ISA Transactions, Volume 51, Issue 3, 2012, Pages 410-419, ISSN , (Article)

[5] N. Kouba, M. Menaa, M. Hasni, M. Boudour. "A novel optimal frequency control strategy for an isolated wind–diesel hybrid system with energy storage devices". Wind Engineering. 2016;40(6):497-517. (Article)

[6] N. Prakash, N. Karuppiah, V. Kumar, R. Vishnu, Z. M. Yousuf "Load Frequency Control of Three Area System using FOPID Controller," WSEAS Transactions on Computer Research, vol. 6, pp. 36-42, 2018 (Article)

[7] H. Zeynelgil, A. Demiroren, N. Sengor "The application of ANN technique to automatic generation control for multi area system". Electr. Power Energy Syst. 2002, 24, 345–354. (Article)

[8] M. Ismail, A. Bendary "Load Frequency Control for Multi Area Smart Grid based on Advanced Control Techniques" ,Alexandria Engineering Journal, Volume 57, Issue 4,2018,Pages 4021-4032,ISSN 1110-0168, (Article)

[9] S. Dhillon, J. Lather, S. Marwaha, "Multi area load frequency control using particle swarm optimization and fuzzy rules", in: 3rd International Conference on Recent Trends in Computing (ICRTC), 2015, pp. 460–472. (Conference Paper)

[10] S. Priyadharshini, P. Vanitha, "Four area interconnected system on load frequency control using firefly algorithm", Int. J. Adv. Res. Electric. Electron. Eng. 3 (1) (2014), ISSN_NO: 2321-4775. (Article)

[11] A. Pappachen, A. Fathima "Load frequency control in deregulated power system integrated with SMES-TCPS combination using ANFIS controller". Int. J. Electr. Power Energy Syst. 2016, 82, 519–534. (Article)

[12] P. Dash, L. Saikia, N. Sinha "Flower pollination algorithm optimized PI-PD cascade controller in automatic generation control of a multi-area power system". Int. J. Electr. Power Energy Syst. 2016, 82, 19–28. (Article)

[13] N. Bahgaat, M. Ahmed, M. Hassan, F. Bendary. "Load frequency control in power system via improving PID controller based on particle swarm optimization and ANFIS techniques". Int. J. Syst. Dyn. Appl. 2014, 3, 1–24. (Article)

[14] F .Zhang, Q. Li" Deep learning-based data forgery detection in automatic generation control" In Proceedings of the 2017 IEEE Conference on Communications and Network Security (CNS), Las Vegas, NV, USA, 9–11 October 2017; pp. 400–404. (Conference Paper)

[15] A. Ulbig, T. Rinke, S. Chatzivasileiadis, G. Andersson," Predictive control for real-time frequency regulation and rotational inertia provision in power systems". In Proceedings of the 52nd IEEE Conference on Decision and Control, Florence, Italy, 10–13 December 2013; pp. 2946–2953. (Conference Paper)

[16] G. Shankar, V. Mukherjee, "Quasi oppositional harmony search algorithm based controller tuning for load frequency control of multi-source multi-area power system". Int. J. Electr. Power Energy Syst. 2016, 75, 289–302. (Article)

[17] P.N. Topno, S. Chanana, "Non-integer order control for LFC problem of two-area thermal power system with GRC". In Proceedings of the International Conference on Innovations in Electrical, Electronics, Instrumentation and Media Technology (ICEEIMT), Coimbatore, India, 3–4 February 2017. (Conference Paper)

[18] A. A. El-Fergany and M. A. El-Hameed, ``Ef_cient frequency controllers for autonomous two-area hybrid microgrid system using social-spider optimiser," IET Gener., Transmiss. Distrib., vol. 11, no. 3, pp. 637_648, Feb. 2017. (Conference Paper)

[19] C. K. Shiva, V. Mukherjee, "A novel quasi-oppositional harmony search algorithm for automatic generation control of power system", Applied Soft Computing, Volume 35, 2015, Pages 749-765, ISSN 1568-4946, (Article)

[20] S.S. Dhillon, J.S. Lather, S. Marwaha, "Multi objective load frequency control using hybrid bacterial foraging and particle swarm optimized PI controller". Int. J. Electr. Power Energy Syst. 2016, 79, 196–209. (Article)

[21] S. Sahoo, S. Sekhar Dash, N. K. Jena, B. K. Sahu, N. C. Patel and R. Bayindir, "SHO designed fuzzy logic based controller for AGC study with capacitor energy storage," 2019 8th International Conference on Renewable Energy Research and Applications (ICRERA), Brasov, Romania, 2019, pp. 845-850, (Conference Paper)

[22] S. Horie, Y. Iwane, K. Kato, T. Goda, K. Yukita, T. Matsumura, Y. Goto "Optimum Frequency Control Method to Counter Prediction Error Effects in Photovoltaic Generators : (Frequency Fluctuation Suppression Method Using Online Adaptive System Constants)," 2018 7th International Conference on Renewable Energy Research and Applications (ICRERA), Paris, France, 2018, pp. 179-183, (Conference Paper)

[23] M. Maaruf, S. E. Ferik, F. S. Al-Ismail, M. Khalid. "Robust Optimal Virtual Inertia Control for Microgrid Frequency Regulation Considering High Renewable Energy Penetration." 2022 11th International Conference on Renewable Energy Research and Application (ICRERA) (2022): 369-373. (Conference Paper)

[24] Kh. Mohammed. Al-Nussairi, D. Sadeq . Al-Majidi, A. R. Hussein, R. Bayindi. "Design of a Load Frequency Control based on a Fuzzy logic for Single Area Networks." 2021 10th International Conference on Renewable Energy Research and Application (ICRERA) (2021): 216-220. (Conference Paper)

[25] Nayak, Smrutiranjan, S. S. Dash, S. K. Kar. "Frequency Regulation of Hybrid Distributed Power Systems Integrated with Renewable Sources by Optimized Type-2 Fuzzy PID Controller." 2021 9th International Conference on Smart Grid (icSmartGrid) (2021): 259-263. (Conference Paper)

[26] Abdul Kader, M. Ozayr, K. T. Akindeji and G. Sharma. "Application of PHEVs Influence on Frequency Regulation of a Two Area Power System." 2022 10th International Conference on Smart Grid (icSmartGrid) (2022): 23-28. (Conference Paper)

[27] H. Li, J. Wang, Z. Du, F. Zhao, H. Liang, and B. Zhou, "Frequency control framework of power system with high wind penetration considering demand response and energy storage," The Journal of Engineering, vol. 2017, pp. 1153-1158, 2017. (Article)

[28] J.G. Ziegler, N.B. Nichols, Optimum settings for automatic controllers, Trans. ASME 64 (1942) 759–768. (Article)

[29] M. Farahani, S. Ganjefar and M. Alizadeh, "PID controller adjustment using chaotic optimization algorithm for multi-area load frequency control," IET Control Theory & Applications, vol. 6, pp. 1984-1992, September 2012. (Article)

[30] K.J. _Astro¨ m, T. Ha¨ glund, Revisiting the Ziegler-Nichols step response method for PID control, J. Process Control 14 (2004) 635–650. (Article)

[31] K. Jagatheesan and B.Anand " Load frequency control of an interconnected three area reheat thermal power systems considering nonlinearity and boiler dynamics with conventional controller" Advances in Natural and Applied Sciences, 8(20) Special 2014, Pages: 16-24. (Article)

[32] B. Abdollahzadeh, F. S. Gharehchopogh, N. Khodadadi, S. Mirjalili, "Mountain Gazelle Optimizer: A new Nature-inspired Metaheuristic Algorithm for Global Optimization Problems", Advances in Engineering Software, Volume 174, 2022, 103282, ISSN 0965-9978, (Article)

[33] P. Trojovský, M. Dehghani," Pelican Optimization Algorithm: A Novel Nature-Inspired Algorithm for Engineering Applications". Sensors 2022, 22, 855. (Article)

[34] M. Mirrashid, H. Naderpour, "Transit search: An optimization algorithm based on exoplanet exploration, Results in Control and Optimization", Volume 7, 2022, 100127, ISSN 2666-7207, (Article)

[35] M. Elsisi , M. Aboelela ,M. Soliman , W. Mansour . "Design of optimal model predictive controller for LFC of nonlinear multiarea power system with energy storage devices" Electr Power Compon Syst. 2018;46:1300-1311.

[36] S. Patel, B. Mohanty, and H. M. Hasanien, ``Competition over resources optimized fuzzy TIDF controller for frequency stabilization of hybrid micro-grid system," Int. Trans. Electr. Energy syst., vol. 30, Sep. 2020, Art. no. e12513. (Article)

[37] H. Bevrani "Robust Power System Frequency Control" ISBN 978-0-387-84877-8 , 2009 (Book)

[38] Y. Arya, N. Kum. "BFOA-scaled fractional order fuzzy PID controller applied to AGC of multi-area multisource electric power generating systems". Swarm Evol Comput. 2017;32: 202-218. (Article)

[39] M. Farahani, S. Ganjefar and M. Alizadeh, "PID controller adjustment using chaotic optimization algorithm for multi-area load frequency control," IET Control Theory & Applications, vol. 6, pp. 1984-1992, September 2012. (Article)

[40] K.J. Astro¨ m, T. Ha¨ glund, Revisiting the Ziegler-Nichols step response method for PID control, J. Process Control 14 (2004) 635–650. (Article)

[41] C. S. Rao. "Adaptive Neuro-Fuzzy Based Load Frequency Control of Multi-Area System under Open Market Scenario". IEEE- International Conference on Advances in Engineering, Science and Management (ICAESM -2012) March 30, 31, 2012. 5-10. (Conference Paper)

[42] B. Sandeep, T. Barjeev, H. O. Gupta. "Genetic algorithm-based PID controller design for a multi-area AGC scheme in a restructured power system". International journal of engineering, science and technology 2011; 3 (1): 220-236. (Article)

[43] H.D. Mathur, H.V. Manjunath, Frequency stabilization using fuzzy logic based controller for multi-area power system, South Pacific J. Nat. Sci. (2007) 22–30. (Article)

[44] Y.H. Song, A.T. Johns, Applications of fuzzy logic in power systems: part 1 general introduction to fuzzy logic, Power Eng. J. (1997) 219–222. (Article)

[45] Y.H. Song, A.T. Johns, Applications of fuzzy logic in power systems: part 2 comparison and integration with expert systems, neural networks and genetic algorithms, Power Eng. J. (1998) 185–190. (Article)

[46] Y.H. Song, A.T. Johns, Applications of fuzzy logic in power systems: part 3 example applications, Power Eng. J. (1999) 97–103. (Article)